

A Polyoxometalate Cluster Paradigm with Self-Adaptive Electronic Structure for Acidity/Reducibility-Specific Photothermal Conversion

Chen Zhang,[†] Wenbo Bu,^{*,†,§} Dalong Ni,[†] Changjing Zuo,[‡] Chao Cheng,[‡] Qing Li,[†] Linlin Zhang,[†] Zheng Wang,[†] and Jianlin Shi^{*,†}

[†]State Key Laboratory of High Performance Ceramics and Superfine Microstructure, Shanghai Institute of Ceramics, Chinese Academy of Sciences, Shanghai 200050, P.R. China.

[§]Shanghai Key Laboratory of Green Chemistry and Chemical Processes, School of Chemistry and Molecular Engineering, East China Normal University, Shanghai 200062, P.R. China.

[‡]Department of Nuclear Medicine, Changhai Hospital, Shanghai 200433, P.R. China.

1. Supplementary Methods

Electrochemical Measurements. Cyclic voltammograms were measured with a standard three-electrode system controlled by a Solartron 1287 electrochemical interface analysis instrument. A platinum sheet (3.63 g, 99.9995%) and an Ag/AgCl (in 3 M KCl solution) electrode were used as the counter electrode and the reference electrode, respectively. To prepare the working electrode, 10 mg of sample POM-*Ox* (POM at oxidation state) was dispersed in 200 μl of water, then mixed with 50 μl of Nafion solution (5 wt % in ethanol) with continuous sonication for 10 min. Subsequently, 10 μl of this solution (containing 0.4 mg of POM-*Ox*) was drop-casted onto a 3 mm diameter glassy-carbon electrode and then the solvent was evaporated at room temperature. All electrochemical measurements were conducted in 50 ml of 0.5 M H_2SO_4 solution with a scan rate of 50 mV s^{-1} .

Dielectric characterization. For the characterization of the dielectric properties, each sample of 0.5 g powders was compacted into pellets that were 12 mm in diameter and about 1.2 mm in thickness with a 10-MPa pressure, and then the face-to-face 5-mm-diameter silver electrodes were coated on both faces of the pellets by using an electric beam evaporation deposition device (DZS-500, Shenyang Scientific Instruments Research Center Co., Ltd., China). Subsequently, the frequency-dependent relative dielectric constant (ϵ_r) at room temperature from 40 to 10^8 Hz was measured by an Agilent HP4294A impedance analyzer equipped with the 16451B test fixture at a bias voltage of 0.5 V.

Cell culture. NRK-52E rat renal proximal tubular cell line and MCF-7 human breast adenocarcinoma cell line were cultured in high-glucose DMEM (Gibco, USA), containing 10% heat-inactivated fetal bovine serum (FBS), streptomycin (100 mg ml^{-1}) and penicillin (100 units ml^{-1}) at 37 °C in humidified atmosphere with 5% CO_2 , endowing the same condition to BRL-3A rat liver cell line and 4T1 mouse breast tumor cell line cultured in RPMI 1640 (Gibco, USA). All the cell lines were purchased from Shanghai Institute of cells, Chinese Academy of Sciences. Cells with different oxygen tension were obtained by culturing them in aerobic incubator (21% O_2) and anaerobic incubator (2% O_2), respectively.

Tumor model. Female Balb/c mice at 7 weeks of age (~ 20 g) were purchased from Shanghai Laboratory Animal Center, Chinese Academy of Sciences. All animal experiments operations were

performed in accordance with the protocols approved by Institutional Animal Care and Use Committee (IACUC) and the care regulations approved by the administrative committee of laboratory animals of Fudan University. Unitary 4T1 tumor-xenografted mice were obtained by being inoculated subcutaneously (s.c.) with 1×10^6 4T1 cells suspended in 100 μ L of PBS in the right thigh. Tri-4T1-tumors bearing mice were obtained by being inoculated subcutaneously (s.c.) with 1×10^6 4T1 cells suspended in 60 μ L of PBS on the back in triplicate at equal distance of 1.5 cm with each other. Then these mice were fed until the tumor volume reached 100 - 130 mm³ (10 days after tumor inoculation).

In vitro Cytotoxicity test. NRK-52E rat renal proximal tubular cells line, BRL-3A rat liver cells and MCF-7 human breast adenocarcinoma cells were seeded in 96-well plates (100 μ L containing 3000 cells per well) and incubated for 24h to attach onto the plate. Then the medium was replaced with fresh culture medium containing either POM-Ox or POM-R4 at Mo concentration of 50, 100, 200, 500 μ g ml⁻¹. After further incubation for 48 h, a typical 3-[4,5-dimethylthiazol-2-yl]-2,5-diphenyltetrazolium bromide (MTT) reduction assay was used to evaluate the cell viabilities relative to the control group. In brief, the cells were mildly washed with PBS for three times, then co-incubated with MTT solution (0.6 mg ml⁻¹ in 100 μ L of FBS-free medium per well) in 5% CO₂ at 37 °C for 4 h. Subsequently, the MTT solution was replaced by 100 μ L of dimethyl sulfoxide (DMSO), and the absorbance was tested on a microplate reader (Bio-TekELx800, USA) at the wavelength of 490 nm. Note that the as-synthesized POM-R4 nanoclusters were used for the subsequent photothermal therapy study *in vitro* and *in vivo*.

Confocal fluorescence imaging. MCF-7 cells were seeded (1×10^5 cells in 1 ml DMEM) respectively in four CLSM-exclusive culture disks and allowed to adhere overnight. Then, these four groups were respectively treated with 1 ml fresh medium replacement (Control group), 1 ml fresh medium containing POM replacement (50 μ g Mo ml⁻¹, POM group), 808-nm NIR laser irradiation (1.5 W cm⁻², 5 min) after 1 ml fresh medium replacement (NIR group) and 808-nm NIR laser irradiation (1.5 W cm⁻², 5 min) after 1 ml fresh medium containing POM replacement (POM + NIR group). After the treatment administration, the media were then replaced by 1 ml of PBS containing 2 μ M Calcein-AM and 4.5 μ M propidium iodide (PI). After incubation at 37 °C in 5% CO₂ for 20 min, the cells were washed with PBS for three times, further detected the fluorescence of Calcein (λ_{ex} = 490 nm, λ_{em} = 515 nm) and PI (λ_{ex} = 535 nm, λ_{em} = 617 nm) to

evaluate the viability of the cells. Separably, the inviable cells (red color fluorescence) were stained by PI, and the viable cells (green color fluorescence) were stained by Calcein.

In vitro specificity of photothermal therapy. MCF-7 cells were seeded (1×10^4 cells in 2 ml DMEM) in eight culture disks and allowed to adhere overnight. After the culture medium of four disks was replaced by 2 ml of fresh medium and 2 ml of medium containing POM ($50 \mu\text{g Mo ml}^{-1}$) for another four, these cells (two disks containing fresh medium and two disks containing POM) were cultured in aerobic incubator (21% O_2) and anaerobic incubator (2% O_2) for 12 h, respectively. Subsequently, similar to the divided groups used in the confocal fluorescence imaging experiment, the NIR group and POM + NIR group were irradiated under 808-nm laser (1.5 W cm^{-2}) for 5 min with an infrared thermal camera (FLIR T420, FLIR Systems, Inc, USA) to monitor the temperature. Afterward, the cells were washed, trypsinized, harvested, resuspended in 100 μl binding buffer and stained by adding 2 μl PI for 20 min in the dark. The stained cells with different treatments were analysed to assess the inviability rate by flow cytometry (EPICS XL/XL-MCL, Beckman, USA) after diluted with 400 μl binding buffer.

In vivo toxicity assay. 15 female Balb/c mice at 7 weeks of age were randomly divided into three groups: control, 7 days treated and 30 days treated mice, respectively. At the corresponding time node after the intravenous (i.v.) injection of an 80 mg Mo kg^{-1} dosage of POM (in 150 μl saline), these mice were sacrificed to collect the major organs (heart, liver, spleen, lung, kidney and brain) for pathological studies by the typical hematoxylin and eosin (H&E) staining assay, with an equal volume of saline intravenously injected mice as control. During this period, the liveweight was recorded every two days to monitor the potential influences of POM on the bodily functions.

Pharmacokinetic study

Measurement of blood clearance. Three female Balb/c mice at 7 weeks were injected intravenously with 100 μl of POM (30 mg Mo kg^{-1} , in saline). Subsequently, 20 μl blood was collected from the tail vein in the indicated time points (5 min, 10 min, 30 min, 1 h, 2 h, 4 h, 8 h, 24 h, 40 h and 72h) and diluted to 4 ml of ultrapure water with 10 mM ethylenediaminetetraacetic acid disodium salt (EDTA-2Na) as anticoagulant. Then ICP-OES was used to determine the time-dependent concentration of Mo in blood. Origin was used for data analysis for the best-fit line and blood terminal half-life based on the two-component pharmacokinetic model.

Urinary and fecal clearance. Female Balb/c mice at 7 weeks were injected with 100 μl of POM

(30 mg Mo kg⁻¹, in saline) via tail vein. For the measurement (n = 3) of the time-dependent concentration variation of POM in excretion, after a mild stimulation performed by gingerly lifting the mouse by its tail in the indicated time points (1 h, 4 h, 8 h post-injection during the first day and once per day for the following 7 days), 50 µl of fresh urine and post-weighed feces samples were then collected respectively via the micturition reflex and defecation reflex. For the evaluation (n = 3) of the accumulative clearance, the mice after injection were placed in metabolic cages, the corresponding urine and feces samples were totally collected respectively once per day for the following week. The Mo content was measured by ICP-OES after the obtained urine and feces samples were digested with aqua regia (V_{HCl} : V_{HNO3} = 3:1). The general equation for the accumulative clearance versus the time (day) (AC_d , % ID) of POM in the excretion (urine or feces) is described as:

$$AC_d = \frac{\sum_{i=1}^d m_i}{m_{ID}} \times 100\%$$

where m_i is the total mass of Mo in the excretion collected at i th day, and the constant m_{ID} is the injected dose of Mo.

Biodistribution. Female Balb/c mice (~ 20 g) bearing 4T1 tumors were injected intravenously with POM (30 mg Mo kg⁻¹, in 100 µl of saline) via tail vein (n = 3 for each group). Mice were sacrificed and the major organs (heart, liver, spleen, lung, kidney, tumor and brain) were collected in six time points (0.5 h, 1 h, 3 h, 24 h, 48 h and 7 days) after injection. These obtained samples were weighted and then digested with aqua regia for ICP-OES analysis of Mo content. The percentage injected dose per gram (% ID g⁻¹) organ/tissue (D) of Mo was calculated by the following equation:

$$D = \frac{m_{Mo} / m_{organ}}{m_{ID}} \times 100\%$$

where m_{Mo} (ug) is the mass in corresponding organ whose mass is m_{organ} (g), and the constant m_{ID} (ug) is the injected dose of Mo. The time-dependent Mo content in heart and tumor was fitted to a first-order model.

In vivo PA imaging. PA/US coregistered images and PA spectra were acquired with a Vevo LAZR instrument (FUJIFILM VisualSonics) equipped with a Vevo imaging station, an anesthesia system,

a LZ400 linear array transducer (18-38 MHz, 256 elements) and a tunable Nd:YAG laser system (OPOTEK Inc., Carlsbad, CA, 5 ns pulse width, 50 mJ pulse peak energy). 4T1 tumor bearing mice were firstly anesthetized using 2% isoflurane in oxygen. PA imaging was performed at multi-wavelength from 680 to 950 nm before injection and in 5 min, 10 min, 0.5 h and 1 h post-i.v. injection of POM (30 mg Mo kg⁻¹). For oxygen saturation (sO₂) estimates, images were acquired using 'Oxyhemo' mode, which collects PA data at 750 and 850 nm and creates a parametric map of estimated oxygen saturation and total haemoglobin at a rate of 1 Hz. The focal depth for all photoacoustic signal collection was set at 11 mm. All the PA signal measurements of region of interest (ROI) and PA image analysis were performed by using the Vevo LAZR imaging system software package.

Tumor distribution in vivo. The fresh dissected 4T1 tumor collected in 1 h post-injection was fresh frozen by immersion in liquid nitrogen to avoid further diffusion of POM, dried under vacuum and then embedded in paraffin. The paraffin block was sectioned in the middle of the tumor so as to obtain the largest tissue area. Immediately, the fresh tumor section was analyzed by X Series II ICP-MS (Thermo Fisher, USA) equipped with a LSX-213 Nd:YAG Laser Ablation System (CETAC Technologies, USA). For the imaging of POM in tumor, Surfer 8 software was used for mass spectral processing and reconstitution of the ⁹⁵Mo ion mapping.

2. Supplementary Figures and Tables

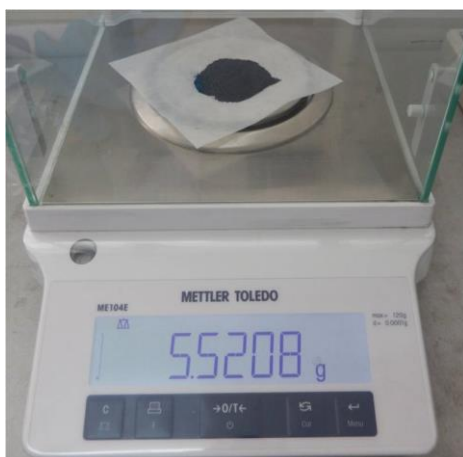


Figure S1. Photograph of the as-synthesized POM nanocluster (**R4**) powders showing more than 5 g of production in one batch of synthesis in a 100 ml beaker.

Table S1. Atomic contents of Mo, P, Na and N in POM nanocluster (**R4**) powder calculated from XPS results (n = 5, mean \pm s.d).

Element	Mo	P	Na	N
Content (atomic %)	25.8 ± 1.7	2.1 ± 0.3	1.6 ± 0.7	5.5 ± 1.1

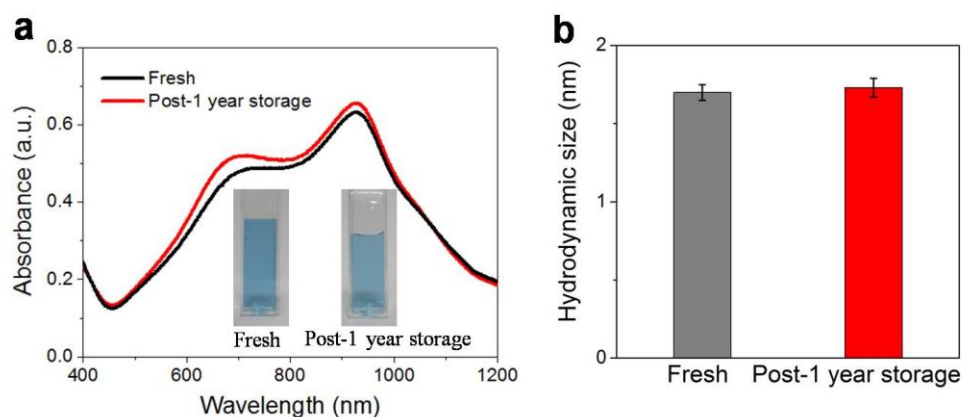


Figure S2. Stability evaluation of POM clusters dispersed in PBS solution (pH = 7.4, 100 ppm Mo) at room temperature for one year sealed storage. (a) UV-Vis absorption of POM nanocluster solution before and after one year storage, showing their outstanding storability with negligible change in the absorption. Note that the observed little enhancement in the absorbance is due to the solvent evaporation during the measurement. The insert is the corresponding digital photos. (b) DLS results comparing POM sizes in the solution before and after one year storage, confirming the excellent stability of POM nanocluster solution even in a high ionic strength PBS medium ($n = 3$, mean \pm s.d).

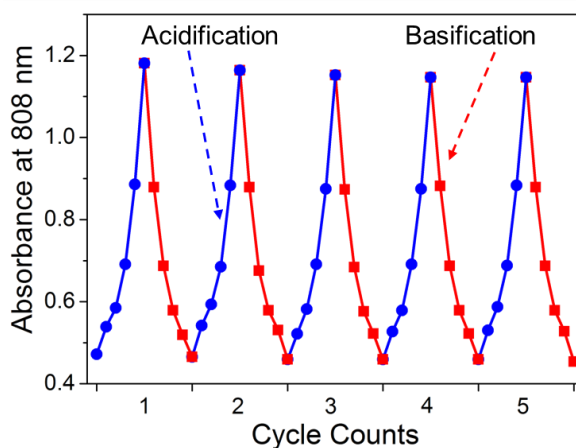


Figure S3. Absorbance value at 808 nm recorded for cyclic acidification and basification of POM nanocluster solutions (100 ppm Mo) at recycling pH values of 7.4, 7.0, 6.5, 6.0, 5.0 and 4.0, presenting a completely reversible pH-dependent UV-Vis absorption and acidity-enhanced 808 nm absorbance of POM.

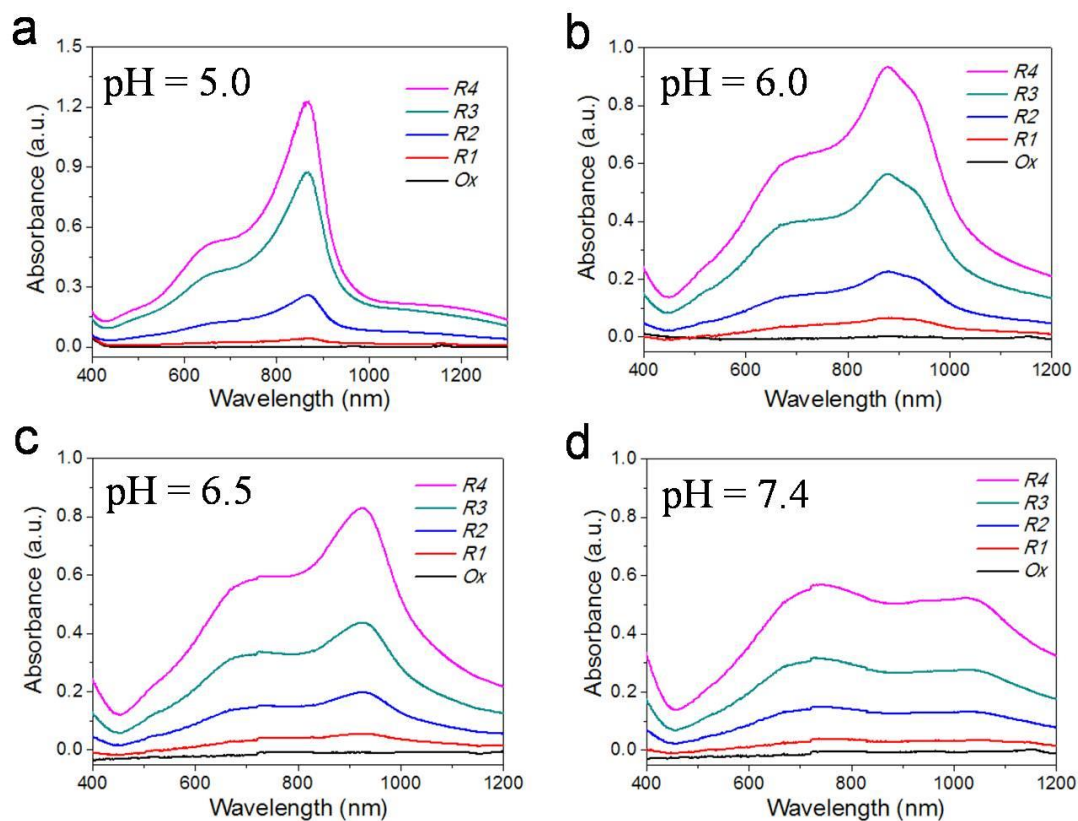


Figure S4. UV-Vis absorptions of POM clusters (100 ppm Mo) dispersed in solutions of various pH values of pH = 5.0 (a), pH = 6.0 (b), pH = 6.5 (c) and pH = 7.4 (d) in responses to the increasing reduction level.

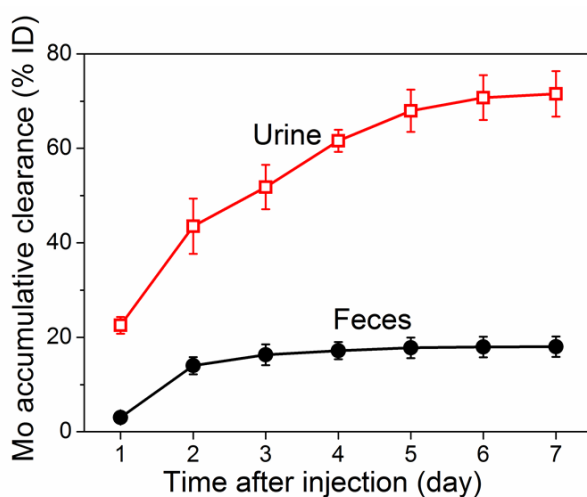


Figure S5. Accumulative clearance of POM through urinary and fecal routes of mice after i.v. injection (n = 3, mean \pm s.d.).

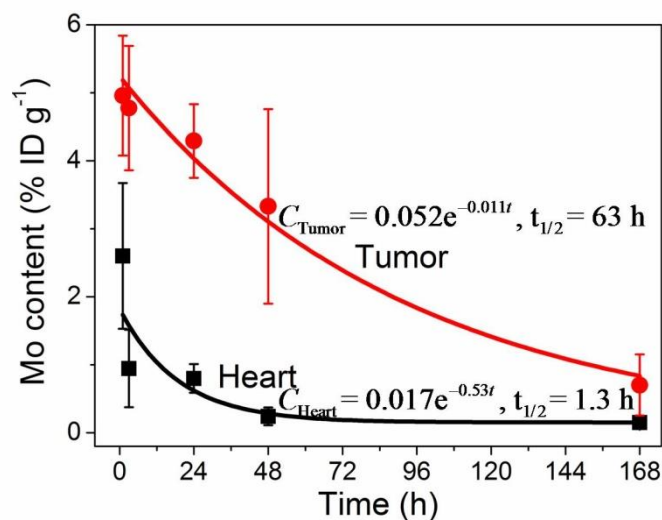


Figure S6. Comparison of POM's clearance rate between tumor and heart, showing a much more significant retention effect of POM in tumor compared to the non-reticuloendothelial heart ($n = 3$, mean \pm s.d), which benefits from a more efficient EPR effect due to the selective self-assembly of the isolated POM clusters in the acidic tumor microenvironment.

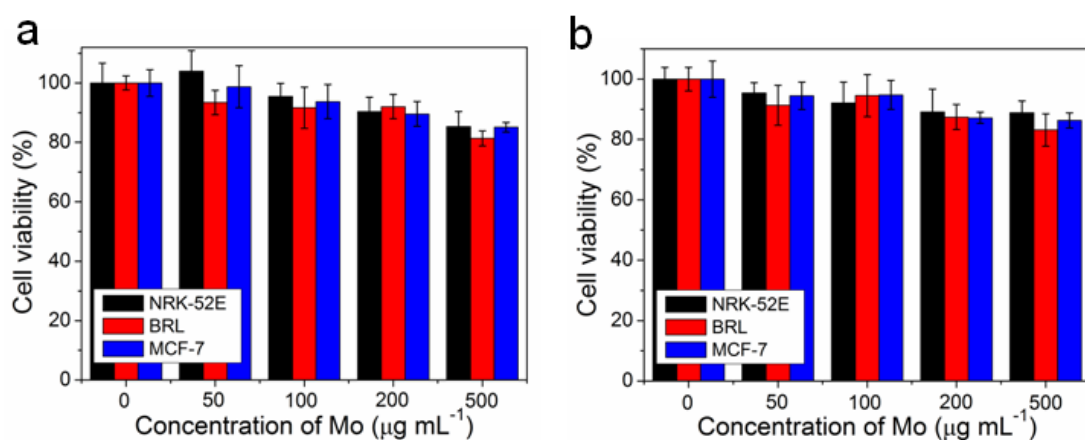


Figure S7. Cytotoxicity assessment of POM. Cell viabilities of NRK-52E (rat renal proximal tubular cell line), BRL (rat liver cell line) and MCF-7 (human breast adenocarcinoma cell line) cells after incubations with POM-*Ox* (oxidation state, **a**) and POM-*R4* (deep-reduction state, **b**) at Mo concentrations of 50, 100, 200 and 500 $\mu\text{g mL}^{-1}$ for 48 h, respectively ($n = 6$, mean \pm s.d). The cell viability remains higher than 85% in each case, indicating negligible cytotoxicity of POM.

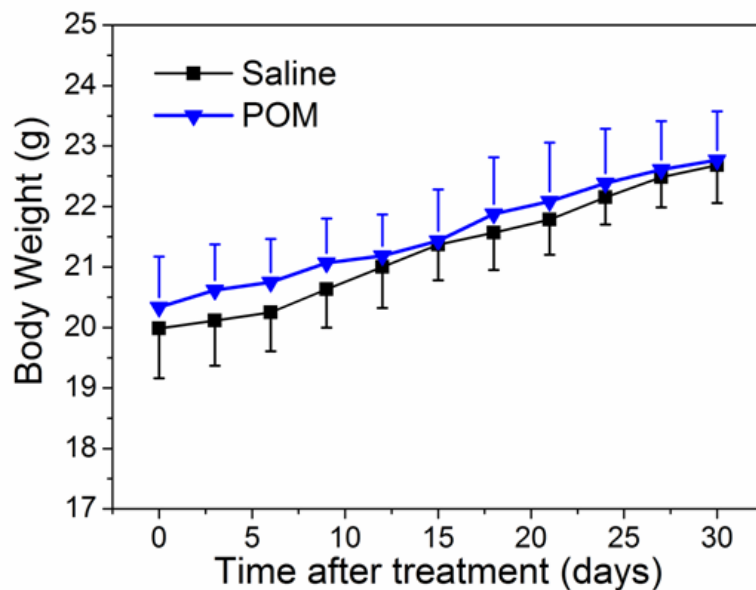


Figure S8. Time-dependent body weight records of Balb/c mice within one month treated with i.v. injection of POM (80 mg Mo kg⁻¹, in 150 µl saline) in comparison to the control (150 µl saline, n = 5, mean ± s.d), showing no significant difference in body weight.

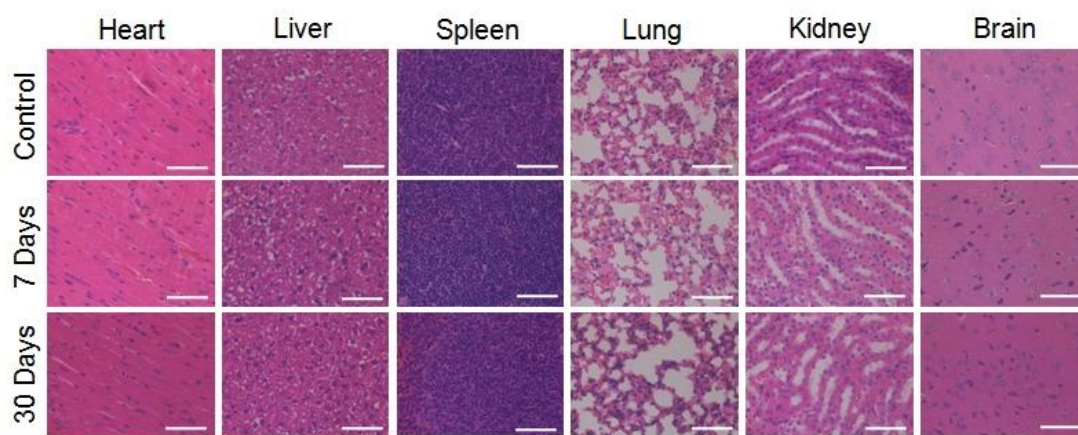


Figure S9. Pathological images of H&E stained tissue sections from heart, liver, spleen, lung, kidney and brain of Balb/c mice, harvested in 7th and 30th day after i.v. injection of a 80 mg Mo kg⁻¹ dosage of POM, showing their good biocompatibility with no detectible acute and chronic toxicity on the main organ. Scale bars, 50 µm.

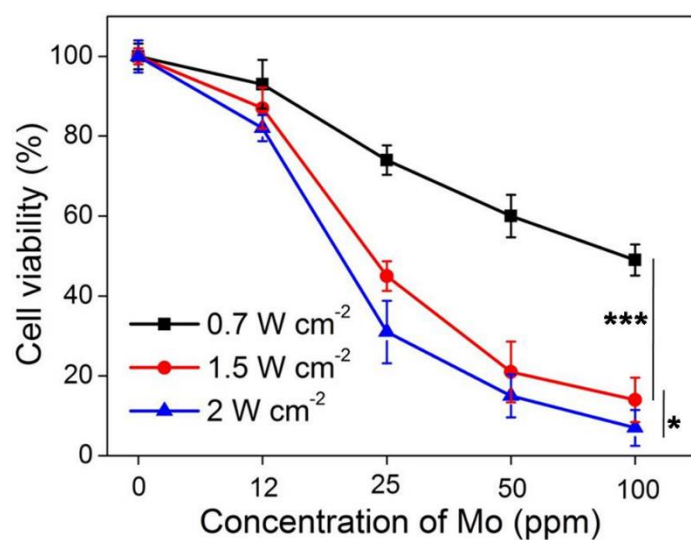


Figure S10. Viability of MCF-7 cells by photothermal therapy at varied concentrations of POM and under 808-nm NIR laser irradiation of varied power densities (0.7, 1.5 and 2.0 W cm⁻², n = 6, mean ± s.d., * P < 0.05, *** P < 0.001).

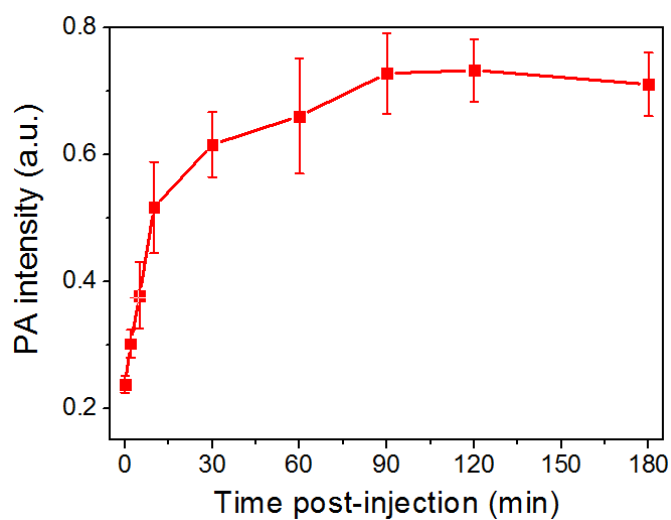


Figure S11. Time-dependent average PA intensity of a subcutaneous 4T1 tumor of a living mouse after i.v. injection of POM (30 mg Mo kg⁻¹). n = 3, mean ± s.d.

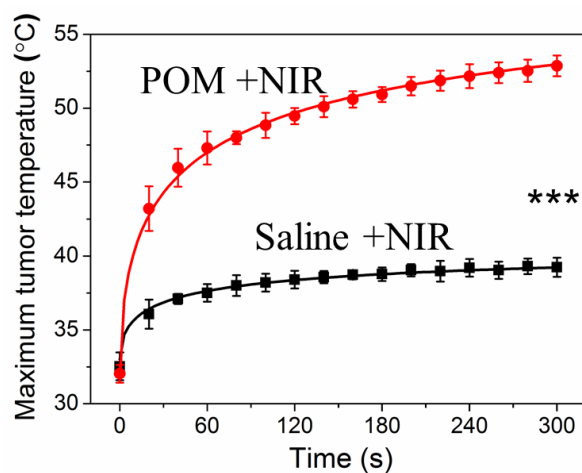


Figure S12. Time-dependent records of the maximum tumor temperature during 808-nm laser irradiation for 5 min ($n = 5$, mean \pm s.d., *** $P < 0.001$).

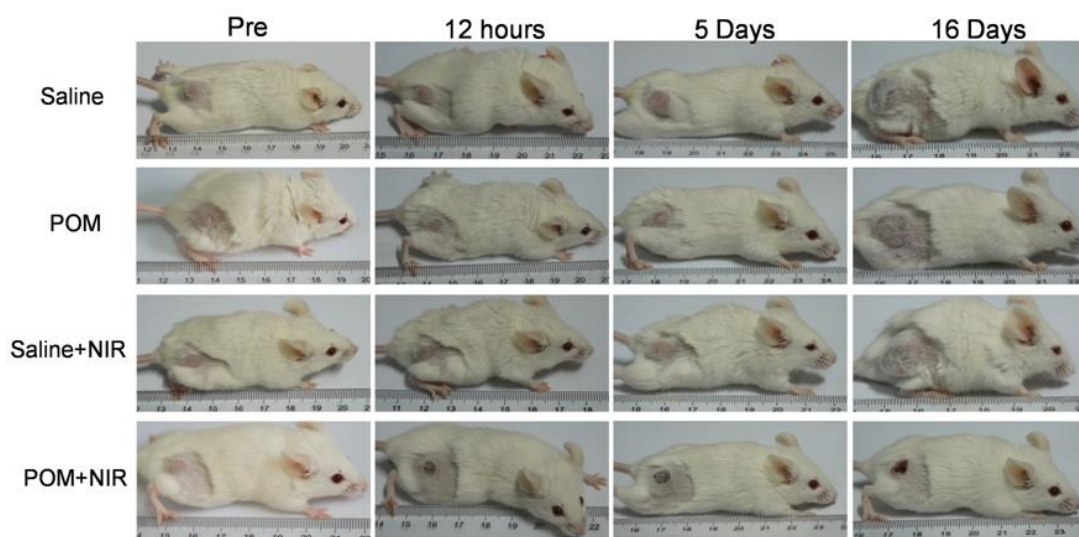


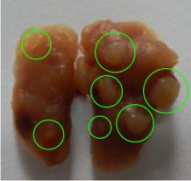



Figure S13. Representative photographs of 4T1 tumor-xenografted Balb/c mouse showing tumors in four treatment groups containing i.v. injection of saline (150 μ l saline), i.v. injection of POM (30 mg Mo kg^{-1} , in 150 μ l saline), under irradiation of 808-nm NIR laser (1.5 W cm^{-2} , 5 min) after 1h-post i.v. injection of saline and POM in 12 h, 5 and 16 days after treatments, revealing an efficient inhibition effect on tumor growth within 16 days through an i.v. administration of POM.

Table S2. Proportion of mice with detected metastatic nodules in the lung on 16th day post-different treatments (n = 5 for each group). The green circle highlights the metastatic nodules. ^aStatistic calculation of the specimens with detected metastatic nodules (mean \pm s.d.). ^bDiameter of the metastatic nodules (mean \pm s.d.).

Group	Saline	POM	Saline + NIR	POM + NIR
Representative photo of metastatic nodules in the lung				
Proportion	4/5	4/5	5/5	0/5
Number ^a	5 \pm 2	2 \pm 2	5 \pm 3	N/A
Size (mm) ^b	1.9 \pm 1.3	2.1 \pm 0.8	2.3 \pm 1.5	N/A

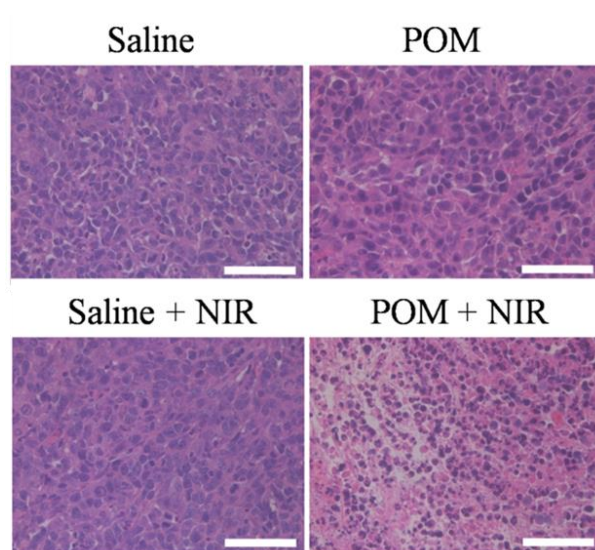


Figure S14. Images of hematoxylin and eosin (H&E) stained 4T1 xenograft tumour tissue sections in the four groups collected in 2h post-treatments. Scale bars, 50 μ m.

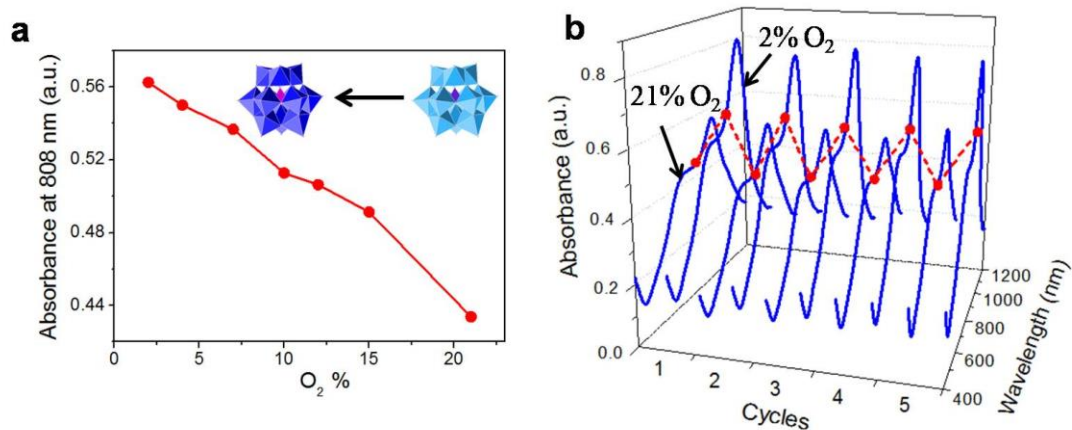


Figure S15. Self-adaptive UV-Vis absorption of POM nanocluster solution. (a) Absorbance at 808 nm of POM nanocluster solution (100 ppm Mo, pH = 6.5) openly placed in the atmospheres of different oxygen concentrations for 6 h. (b) UV-Vis absorption of POM nanocluster solution during the cyclic stroages in 21% O₂ and 2% O₂ atmospheres. The red dash line highlights their cyclic change of absorbance at 808 nm.

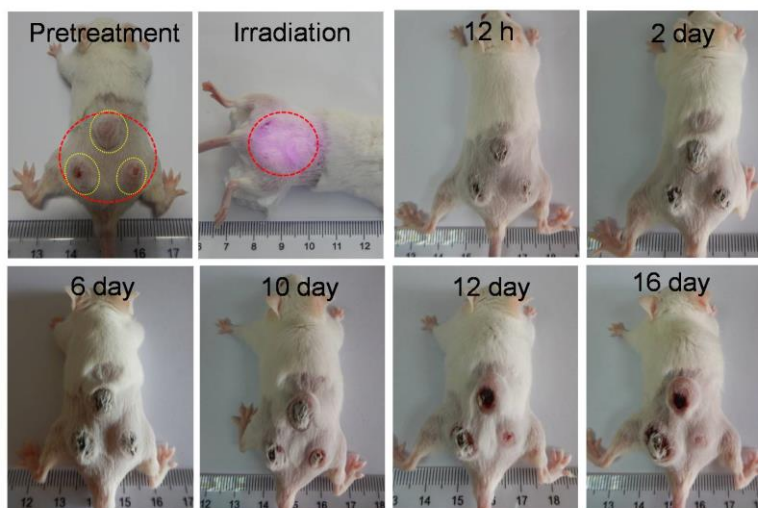


Figure S16. Representative photographs of a tri-4T1-tumors bearing Balb/c mouse experiencing an expanded 808-nm laser irradiation (1.5 W cm^{-2} , 5 min) after i.v. injection of POM (30 mg Mo kg^{-1}). The yellow circles mark the three tumors on the back. The red circle highlights the irradiated region. Note that the upper tumor is part-covered in the 808-nm laser irradiation.

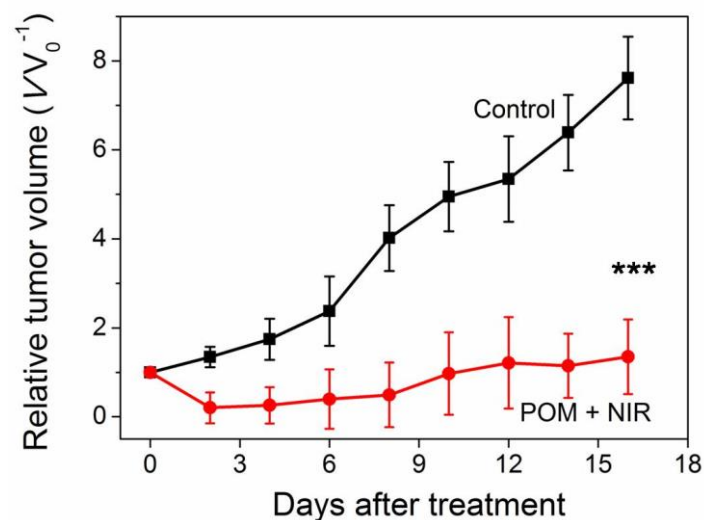


Figure S17. Time-dependences of relative tumor volumes in the tri-4T1 tumour-bearing mice treated with i.v. injection of saline (Control) and 808-nm laser irradiation in 1 h post- i.v. injection of POM (POM + NIR). $n = 9$, mean \pm s.d. The proof-of-concept POM induced specific photothermal therapy by the expanded large-area 808-nm laser irradiation shows a significant inhibition on the tumor growth. In contrast to the complete tumor eradication for all the tumors observed in the non-expanded 808-nm laser irradiation, the therapeutic difference on the three tumors is due to the limit of the expanded 808-nm laser setup, which could hardly ensure the same irradiation dose on the individual tumor originated from the uneven energy distribution after using the beam expander. A ring array of 808-nm NIR lasers should be a much better irradiator for the large-area laser irradiation with the uniform energy distribution.